Biochimica et Biophysica Acta 1798 (2010) 730–740

Contents lists available at ScienceDirect

Biochimica et Biophysica Acta

journal homepage: www.elsevier.com/locate/bbamem

Review

Surface view of the lateral organization of lipids and proteins in lung surfactant model systems—A ToF-SIMS approach

Mohammed Saleem [1], Hans-Joachim Galla *

Institute of Biochemistry, University of Münster, Wilhelm-Klemm-Str. 2, 48149 Münster, Germany

ARTICLE INFO

Article history:
Received 29 July 2009
Received in revised form 12 October 2009
Accepted 14 October 2009
Available online 29 October 2009

Keywords:
Time-of-flight secondary ion mass spectrometry
Chemical imaging
Surfactant protein B
Lung surfactant
Lipid–protein interaction
Lateral organization of membrane

ABSTRACT

The lateral organization of domain structures is an extremely significant aspect of biomembrane research. Chemical imaging by mass spectrometry with its recent advancement in sensitivity and lateral resolution has become a highly promising tool in biological research. In this review, we focus briefly on the instrumentation, working principle and important concepts related to time-of-flight secondary ion mass spectrometry followed by an overview of lipid/protein fragmentation patterns and chemical mapping. The key issues addressed are the applications of time-of-flight secondary ion mass spectrometry in biological membrane research. Additionally, we briefly review our recent investigations based on time-of-flight secondary ion mass spectrometry to unravel the lateral distribution of lipids and surfactant proteins in lung surfactant model systems as an example that highlights the importance of fluidity and ionic conditions on lipid phase behavior and lipid–protein interactions.

Contents

1. Introduction

The molecular mechanisms underlying lipid–protein interactions are highly significant for studies of structure–function relationship in membranes. In particular, biological processes in which specific lipids are required for proper functioning has attracted much research. One such phenomenon, where specific lipid–protein interactions become indispensable, is to facilitate a continuous and effortless breathing process.

The alveolar interface is lined by a complex mixture of phospholipids and surfactant proteins, whose interplay works to reduce the surface tension at the alveolar surface, thereby, preventing alveolar collapse [1,2]. A significant amount of knowledge has been acquired on the physiological importance of lung surfactant in premature neonates and adults[3,4], and the role of phospholipids, surfactant proteins and their model peptides [5–12] on phase behavior [13–16] and their structure–function relationship [17–19]. The major phospholipid constituent of pulmonary surfactant is the phosphatidylcholine (PC),

* Corresponding author. Tel.: +49 251 8333200; fax: +49 251 8333206.
E-mail address: gallah@uni-muenster.de (H.-J. Galla).
[1] Present address: Physico-Chemistry Curie, Institute Curie, Paris, France.

0005-2736/$ – see front matter © 2009 Elsevier B.V. All rights reserved.
doi:10.1016/j.bbamem.2009.10.011

especially dipalmitoylphosphatidylcholine (DPPC) [20–22]. DPPC plays an important role in reducing surface tension to very low values and thus protecting the alveolus against collapse [2,23,24]. Other lipids that are essential for lung surfactant function are the anionic phosphatidylglycerol (PG), and phospholipids containing unsaturated acyl chains [22,25]. Besides phospholipids, surfactant proteins namely SP-A, SP-B, SP-C, and SP-D, have been found to be of immense importance in assembly and functioning of the lung surfactant [26–28]. SP-A and SP-D are hydrophilic proteins that play an important role in the storage and transport of lung surfactant and participate in host defense [29], whereas the hydrophobic proteins SP-B and SP-C have been shown to play an important role in promoting/enhancing the adsorption and spreading of monolayers containing large amounts of DPPC.

Attempts to understand the mechanism of surfactant function are numerous. However, the complexity of the system and the technical limitations has impeded its complete understanding. Nevertheless, efficient model systems have been established and studied that seem to closely mimic the properties of native composition. However, observations of specific lipid–protein interactions in various lung surfactant model systems have not been conclusive. To our knowledge, specific SP-B/DPPG interactions were first proposed based on fluorescence anisotropy studies in lipid bilayers [15], and it was proposed that SP-B interacts specifically with PG head groups [17]. Furthermore, electron paramagnetic resonance spectroscopy studies in vesicular systems also suggested preferential interaction between anionic DPPG and SP-B [30]. On the contrary, other bilayer studies based on ^{2}H nuclear magnetic resonance did not observe any preferential interaction of SP-B with either DPPC or DPPG [31]. Surprisingly, our recent monolayer studies based on time-of-flight secondary ion mass spectrometry (ToF-SIMS) imaging demonstrated that both SP-B and its mimetic peptide KL_4 preferentially tend to colocalize with the zwitterionic DPPC. This, however, did not rule out the existence of specific DPPG/protein interactions. Further studies to elucidate the possible influence of the ionic conditions, showed a reversal of surfactant protein colocalization with the anionic DPPG in the absolute absence of calcium ions [32].

In this review, we will mainly focus on the ToF-SIMS imaging as applied in biological systems and particularly its capacity for molecular identification and chemical imaging needed to unravel the lateral organization of membrane structure in model membranes. ToF-SIMS imaging provides a link between the contemporary techniques with atomic scale resolution and the optical microscopy has the unique advantage of providing direct insights into the chemical composition with a resolution down to less than 100 nm. In the following sections, we will briefly describe the working principle of ToF-SIMS, the chemical identification of biomolecules and the lateral organization of lipid–protein membrane systems. Finally, the exploitation of SIMS imaging to characterize the lipid–protein interaction in the lung surfactant model membranes during our studies over the last years will be described.

2. Time-of-flight secondary ion mass spectrometry (ToF-SIMS)—Overview

Time-of-flight secondary ion mass spectrometry (ToF-SIMS) is a powerful technique for high resolution surface, interface and thin film analysis that enables label-free detection of individual components of a monolayer, transferred to a solid support. As shown in Fig. 1, ToF-SIMS involves rastering of a highly energetic electrically focused primary ion beam across the sample inducing a collision cascade that may lead to the release of charged molecules, and compound-characteristic secondary ions fragments [33]. The emitted fragment ions are then accelerated by an electric field in the time-of-flight analyzer leading to separation and detection of the ions according to their mass-to-charge ratios (m/z), thus, offering a high mass range, high mass resolution and a precise mass detection [34,35]. Eventual performance depends on critical factors such as the kind of primary ions source and modulation of its pulses. It is important to note that ToF-SIMS basically is a destructive technique as the highly energetic primary ion beam induces desorption of surface ions. However, use of very low intensity primary ion dose permits quasi-non-destructive analysis. We now briefly describe the primary ions sources: modulation, collision cascade, sputtering process and lateral resolution.

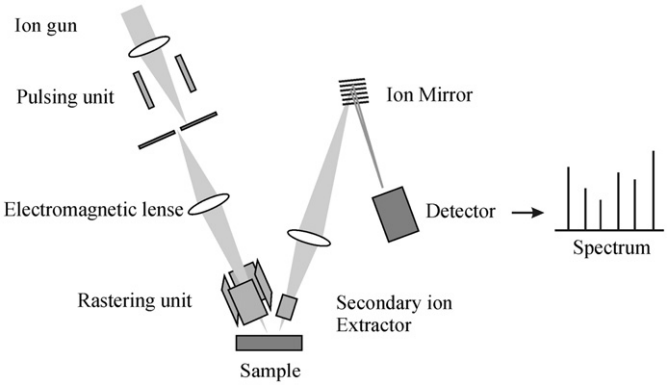

Fig. 1. ToF-SIMS instrumentation. A general scheme of ToF-SIMS showing the important components of the instrumentation.

2.1. Primary ion sources and modulation

The two commonly deployed primary ion sources in biomolecular research are electron impact (EI) sources and liquid metal ion guns (LMIG). Primary ion sources such as polyatomic SF_5^+ and fullerene ion beams (C_{60}^+, C_{60}^{2+}, C_{60}^{3+}) are generated by collision of the gaseous or vaporized source with the accelerated electrons (*electron impact*). The resulting ions have energies in the keV range and offer a significant secondary ion yield. In LMIG's, metals such as gallium, bismuth and gold flow from a reservoir to a small needle tip, thereby establishing a Taylor cone which is then ionized under high voltage to generate stream of metal cations. Bismuth and Gold have recently become the most popular ion source for LMIG's due to their ability to provide not only monoatomic singly charged ions (*like Gallium*) but also cluster of ions such as Bi_3^+, Bi_3^{2+} or Au_3^+ (*unlike Gallium*) [34].

Another essential aspect of ToF-SIMS involves the modulation of the primary ion beam in order to enable high lateral and mass resolution. Spatial focusing or pulsing of the primary ion is done to allow proper separation of secondary ion fragments desorbed off the surface according to there m/z ratio. This is also important to eliminate the varying accelerations of the primary ions resulting from mass and charge discrepancies. There are two kinds of operational modes of the ToF-SIMS which differ in pulse duration and sorting of the primary ions. In "burst alignment mode," the pulsing (10–100 ns), specific mass selection and focusing of the primary ion are optimized to achieve a high lateral resolution of ~ <100 nm [36]. On the contrary, the "bunched mode" involves a significant reduction of the pulse duration to shorter than 1 ns with a bunching device that enables conjunct flow of primary ions and forces primary ions with different speeds to hit the surface at the same time [34]. This allows a mass resolution of >10000 (i.e., $m/\Delta m$) [37]; however, chromatic abberation of the lense system in the bunching device tends to lower the lateral resolution to ~ 2–5 μm [36]. Thus, the above described operational modes could be effectively used to obtain high lateral resolution for chemical imaging of surfaces (*Burst alignment mode*) as well as high mass resolution for acquisition of spectra (*Bunched mode*).

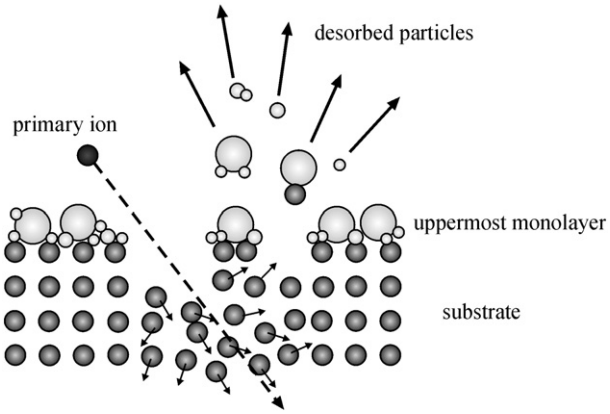

Fig. 2. Collision cascade. A general scheme of the collision cascade from the sputtering of molecular fragments and secondary ions.

2.2. Collision cascade

The primary ion pulse hitting the surface of the sample strikes off largely uncharged fragments and secondary ion fragments attributed to the sample. During this process, the high energy primary ion pulse transfers its kinetics energy to the atoms and molecules of the sample thereby inducing a large scale random collision process and bond breaking as depicted in a simplified scheme of collision cascade in Fig. 2. The collision cascade is isotropic and its range is limited in lateral cross section and longitudinal depth. It is important to recognize that only a small fraction of (10^{-1} to 10^{-6}) of the emitted fragments are either positively or negatively charged and only these fragments can be accurately detected [33,38]. The destructiveness of the ToF-SIMS technique comes from the fact that collision cascades cause the desorption of fragment ions from the surface thereby ablating the region of interest. Nevertheless, ablation and damage of the sample surface can be controlled by ensuring a low primary ion dose and a controlled duration of bombardment. Such a low primary ion dose falls under the "static" SIMS regime in which the damage caused to the sample is negligible and the chemical images of the surface are representative for the sample. The primary ion dose density required for "static" SIMS corresponds to ~ 10^{11}–10^{13} ions/cm^2 and results in the fragmentation of the surface exclusively to a depth of one or at most a few monolayers of the molecular components [39,40]. Conversely, a higher primary ion dose density allows for "dynamic" SIMS in which a continuous removal of the surface ions allows reconstruction of depth profiles of the sample and characterization of elemental components [41,42].

2.3. Detection of secondary ion fragments by time-of-flight analyzer

The subsequent critical step after the induction of collision cascade and sputtering of surface ions is the sorting and detection of the secondary ion fragments by the time-of-flight analyzer based on the respective m/z ratio. This involves acceleration of released secondary ion fragments through a uniform electric field, and depending on the charge of the fragment, the resulting nominal kinetic energies (E_{kin}) is given by [38],

$$E_{Kin} = zV_0e \tag{1}$$

where z denotes the net charge on the secondary ion, e represents the elementary charge and V_0 is the accelerating voltage of the applied electric field. Also, the E_{kin} of an ion is related to its mass (m) and velocity (v) by

$$E_{kin} = \frac{1}{2}mv^2 \tag{2}$$

Thus, the velocity of a given ion is then

$$v = \left(\frac{2E_{Kin}}{m}\right)^{1/2} \text{ or } v = \left(\frac{2zV_0e}{m}\right)^{1/2} \tag{3}$$

Clearly, the mass to charge ratio of each ion depends only upon the ion velocity,

$$\frac{m}{z} = \frac{2V_0e}{v^2} \tag{4}$$

After the initial acceleration, ions enter the drift region and travel over a distance (L) to the detector. The velocity and time of flight (t) are related by

$$v = \frac{L}{t} \tag{5}$$

Substituting Eq. (5) in Eq. (4), we finally get the relation between the m/z ratio of an ion and its time of flight.

$$\frac{m}{z} = \frac{2V_0et^2}{L^2} \tag{6}$$

Since V_0 and L are constant, the flight time (t) is proportional to the square root of the mass of the secondary ion, and as one would expect, the lighter ions travel at a faster velocity and arrive at the detector earlier than the heavier ions.

2.4. Factors crucial for lateral resolution in SIMS imaging

The maximum attainable lateral resolution is a very important feature for any imaging technique. One of the major parameters that define the lateral resolution in ToF-SIMS is the dimensions of the collision cascade that depends both upon the properties of the primary ions (atomicity, energy and mass) and the sample surface (density). For typical primary ion energies, the lateral resolution varies from 2 to 10 nm [42]. The other crucial factor is the spot size of the primary ion focus. While this is usually ~50 nm, de-magnifying beam optics can reduce the spot size and increase the lateral resolution significantly. This is most applicable to thick layers where the primary ion dose can be enlarged. The technical details of the effect of the focus spot size are beyond the scope of this review and can be found elsewhere [42]. The last parameter that needs to be introduced in this regard is the efficiency of secondary ion generation [43]. In particular, in samples where the amount of the secondary ion generated is limited, the secondary ion emission yield is critical for defining the lateral resolution known as the "useful lateral resolution (Δl)." During the acquisition of spectrum, secondary ion emission yield (Y) is defined as the ratio of the number of secondary ions detected (N_D) to the number of primary ions bombarding (N_P) the sample surface

$$Y = \frac{N_D}{N_P} \tag{7}$$

Also, under prolonged bombardment by the primary ion beam, there is a continuous desorption of the secondary ions from the surface defined as the "disappearance cross section (σ)." This process contributes to the exponential decay of the signal intensity of the secondary ion emission given by

$$N_D = N_{D,\,t=0}\exp(-\sigma_D \cdot PIDD) \tag{8}$$

where PIDD denotes the primary ion dose density and the disappearance cross section (σ) is the slope of the exponential decay. The relation between Y and σ explains the concept of "useful

lateral resolution" by the given equation dealt in detail elsewhere [34,42].

$$\Delta l = \left(\frac{N_D \sigma}{Y}\right)^{1/2} \quad (9)$$

2.5. Quantitative limitation

It is important to realize that SIMS is a semi-quantitative technique and quantification remains to be an active area of research in this field. "Dynamic" SIMS can be used to compare the signal from a desired analyte to that of a normalizing component that has a known concentration. Using identical conditions, the SI yield of the unknown component and the normalizing component are measured in both the sample of interest and a reference sample [44]. In contrast, molecular quantification is difficult to achieve in the "static" SIMS. In addition to the surface concentration of the analyte, the chemical environment surrounding the analyte, topology and matrix–analyte interactions, all play an important role in deciphering the acquired intensities of the secondary. This limitation to the SIMS quantification is known as the "Matrix effect" [45,46] and is a matter of active ongoing research. Quantitative information of the sample composition is obtained by calibrating the secondary ion yields against reference standards chosen to have similar ionization potentials and chemical reactivities as the analyte. However, despite the usage of reference species resembling in chemical characteristics, matrix effects corresponding to the changes in the thickness of sample layer might still exist. It has been observed that for a multilayer sample the secondary ion yield is ~ 1.5–5 times lower than the corresponding monolayer surface [46]. Although several potential solutions to the matrix effects have been proposed, such as applying the infinite velocity method found in details elsewhere [47], improvements in matrix effects are still needed.

3. Sample preparation

Because SIMS is a highly sensitive surface analytical tool, sample preparation is crucial for accurate measurement and analysis. Depending on the nature of the sample, preparation can vary from freeze-fractured samples to solid supported samples obtained by Langmuir Blodgett (LB) transfer . The bottom line to any of the above mentioned sample preparation methodology, however, is to allow minimum changes to the native state before the mass spectrometry is carried out under ultrahigh vacuum. The study of membrane structure generally involves the usage of solid supported membranes formed either by LB transfers or adsorption of vesicles to the solid supports. LB transfers involve the spreading of the lipid/protein sample in organic solvents onto an aqueous subphase followed by transfer to solid supports leading to the deposition of uniform and highly ordered membrane layers onto the solid support. Gold coated glass and mica sheets are the typical solid supports because they are atomically flattened surfaces and do not charge up during bombardment [39,48,49]. LB transfers also ensure that the native morphology of the lipid/protein membrane on the subphase is retained upon transfer to the solid support [50,51]. Based on the nature of sample and experimental goals, other widely used sample preparation methodologies are fast-freezing and low temperature dehydration [52,53], chemical fixation, air drying, resin embedding and ultramicrotomy [44,54] the details of which are beyond the scope of this review. Optical microscopy or with high lateral resolution techniques such as scanning force microscopy (SFM) or electron microscopy, should be used to examine samples prior to SIMS imaging to check for any environmental contamination and integrity of the analyte on the substrate. Additionally, these techniques enable further investigations of the same sample using different complementary techniques such as fluorescence microscopy or atomic force microscopy [44].

4. ToF-SIMS in membrane research

Lateral organization of lipids and proteins in biological membranes is an extremely active area of research. While the raft hypothesis suggests the formation of highly organized microdomains enriched in selective lipids and membrane anchored proteins, the direct visualization of so-called "rafts" remains controversial [55]. Phase separated domains are usually imaged using fluorescence dyes that preferentially partition between co-existing lipid phases. However, the precise chemical composition of the domains remains unclear with fluorescence microscopy.

To our knowledge, ToF-SIMS was first applied in biological research in 1978 by Beninghoven et al., who used it for the identification and characterization of biological macromolecules such as peptides, nucleotides and vitamins [56]. The same group subsequently applied this technique to the characterization of the mutant Apolipoprotein A-I along with its variants, by the same group [57,58]. The significant improvements to the lateral resolving power of this technique in the recent years, encouraged us to apply SIMS imaging to investigate the lateral organization of the lung surfactant model membrane, a system which had been well characterized in terms of phase behavior by Langmuir film balance and fluorescence microscopy techniques. We applied ToF-SIMS to investigate the lateral organization of the lung surfactant components and the role of ionic environment to be considered in detail in the later part of this review [46,48,49,59–61]. Furthermore, we showed that, for DPPC/DPPS monolayers, the presence of calcium induces the formation of domains enriched in DPPS. This process may be physiologically important for the interaction of the peripheral membrane protein, annexins [51]. Likewise, ToF-SIMS has been applied extensively to study lateral phase separation, lipid–lipid interaction and lipid–protein interaction in solid supported monolayers and bilayers [62–65]. More recently, domain analysis of monolayers composed of a putative raft mixture sphingomyelin, cholesterol and 1-palmitoyl-2-oleoylphosphatidylcholine (POPC) was characterized with 1 μm lateral resolution that showed the preferential colocalization of sphingomyelin and cholesterol leaving out POPC [66]. A very interesting quantitative chemical mapping by NanoSIMS visualized lipid phase separation at a very high resolution. NanoSIMS is technically different from the conventional SIMS as it involves bringing the primary ion beam normal to the sample surface unlike the typical oblique orientation thereby enhancing resolution [67]. This study on homogeneous solid supported bilayers composed of 1,2-dilauroylphosphatidylcholine-15N (^{15}NDLPC) and 1,2-distearoylphosphatidylcholine- 13C18 ($^{13}C_{18}$-DSPC), showed that domains enriched with $^{13}C_{18}$-DSPC (gel phase) phase separated within a ^{15}NDLPC-rich bilayer [67]. The size (~100 nm in diameter) and the geometries of the phase separated DSPC domains as visualized by NanoSIMS were consistent with atomic force microscopy images. Furthermore, quantitative information on the lipid composition of the membrane was obtained by calibrating the lipid-specific secondary ion signal intensities with reference samples [67].

Similarly, ToF-SIMS has also been applied to study the membrane composition within biological tissues and single cells with a lateral resolution of few microns [34,37,53,68–71]. Particularly interesting reports exploring the potential of this technique showed the selective enrichment of aminoethylphospholipid and selective exclusion of phosphatidylcholine at the fusion junctions of the plasma membrane during mating in *tetrahymena* cells [72]. Likewise, a report from Breitenstein et al. demonstrated a complete generation of chemical maps of animal cells and their intracellular compartments [73]. In the subsequent part of the review, we will describe the fragmentation pattern of each individual component of interest that enables us to assign the so-called fingerprint ions characteristic to a particular lipid or protein. The knowledge of such characteristic secondary ions is essential for the unambiguous mapping of SI signals corresponding to

specific components. We will then review the chemical mapping of lipid–protein lateral organization in the lung surfactant model membranes in detail as determined via ToF-SIMS imaging.

5. Mapping lipid/protein lateral organization

5.1. Identification of biomolecules by their chemical fingerprint ions

Under bombardment by the primary ion, each type of molecule has a characteristic fragmentation pattern that produces a distinctive series of charged ions, the so-called fingerprint ions. Thus, the study of fragmentation of individual molecules is essential for assigning the respective signals in more complex systems and several reference libraries comprising large amounts of spectral data characteristic of organic and macromolecules have been established [74,75]. Fig. 3 presents an example of a ToF-SIMS spectrum of positive SI of DPPC. The primary ion pulse was bunched in order to obtain a high mass resolution (i.e., the nominal mass divided by the difference in mass between the two species ($m/\Delta m$)) needed to distinguish between two adjacent masses with high precision. The various typical fragments attributed to the head group of DPPC correspond to the m/z ratios of 102, 104, 125, 150, 166, 184 and 244 as shown in the schematic picture of the fragmentation pattern of a DPPC in Fig. 4. Additionally, DPPC is found to desorb both as protonated and dehydrogenated quasi-molecular ions $(DPPC+H)^+$ and $(DPPC-H)^+$ with corresponding masses of 732.5 and 734.5 u/e, respectively. The m/z ratios obtained for DPPC correspond well with those obtained by other mass spectrometric techniques [46,76–79]. Fragmentation of the choline head group of DPPC gives rise to the nitrogen-containing SI with m/z ratios less than 100 u/e that sometimes interfere with the non-specific SI in the same m/z regime. However, the problem of interference is overcome during analysis as the intense nitrogen-containing SI gives rise to a peak with even nominal masses due to the presence of lone pair of electrons [43]. On the contrary, intense non-specific SI corresponds to odd masses or hydrogen containing SI. For example, $C_4H_8N^+$ interferes with $^{13}CC_4H_9^+$ and $C_5H_{10}^+$ as they all possess a nominal mass of 70. However, the peaks corresponding to the later are weak due to the presence of lone pair of electrons. Likewise, the ^{13}C isotope contribution could be deduced considering the amount of $C_5H_9^+$ where the amount of ^{13}C corresponds to 1.1%, thus, adding to a total of at least 3% of the intensity of M70 as reported by Bourdos et al. [48]. Most prominent SI fragments corresponding to particular lipids are listed in Table 1.

Mass spectra of lipids are usually rich in signals arising from the acyl chains that are indistinguishable, especially in the lipids containing identical acyl chains. Therefore, it is impossible to differentiate between the acyl signals arising from DPPC and DPPG. Also, anionic lipids such as DPPG do not yield any positive SI fingerprint except the protonated phosphogylcerol $C_3H_{10}PO_6^+$ (M173) that shows a weak signal compared to the overwhelming $C_5H_{15}NPO_4^+$ (M184) ion of the DPPC. Likewise, dipalmitoylphosphatidylglycerol (DPPG) is sometimes detected as a quasi-molecular ion in the form of $(DPPG + 2\ Na\text{-}H)^+$, however, with a very low intensity [80]. Other anionic lipids such as dipalmitoylphosphatidylserine (DPPS) are often detected by the bridging calcium ions or as calcium phosphate [43,51]. This makes it extremely difficult to differentiate the signals arising

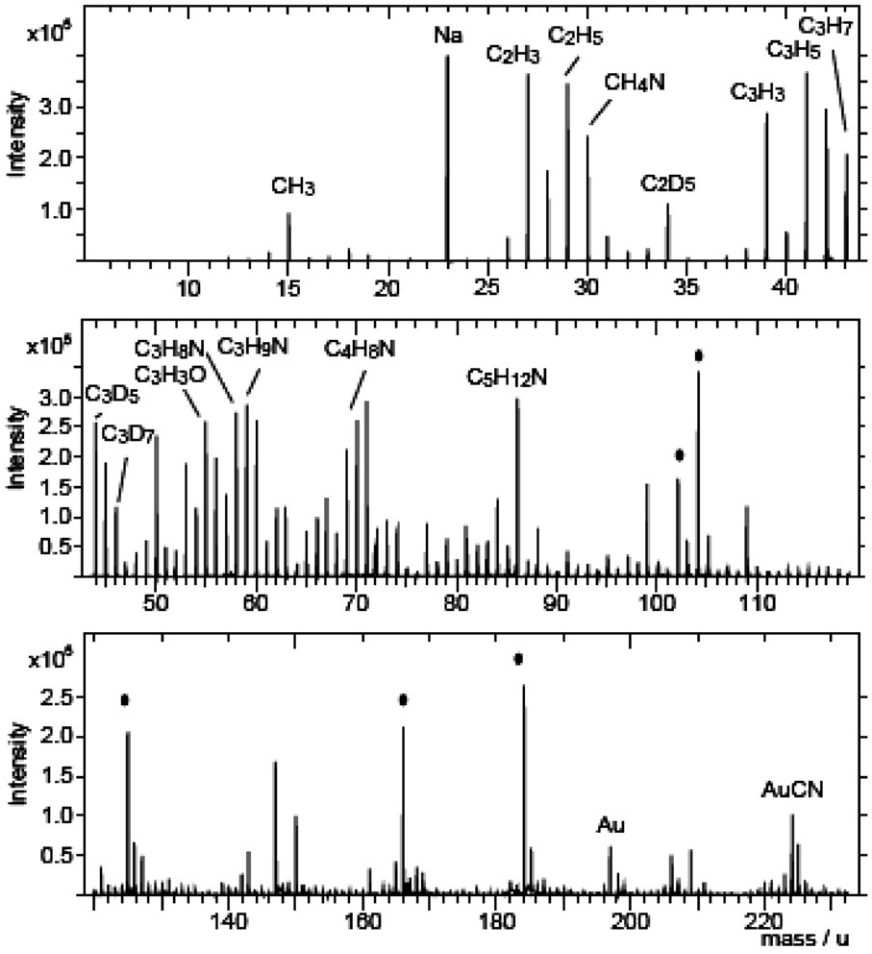

Fig. 3. ToF-SIMS spectrum of DPPC. A mass spectrum showing the positive secondary ions characteristic of DPPC.

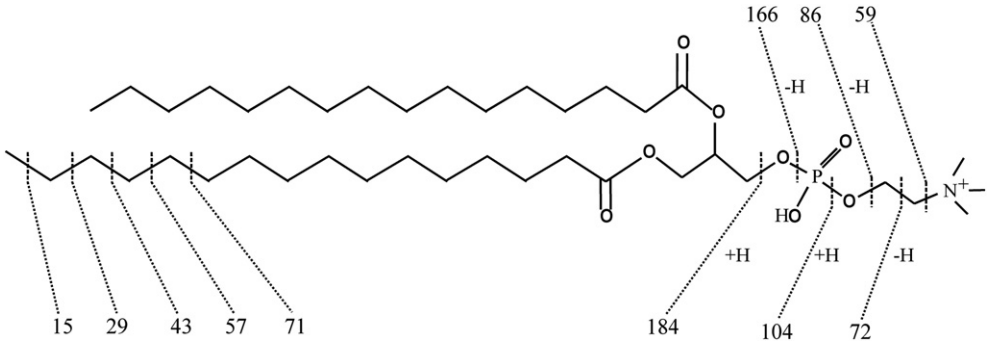

Fig. 4. Fragmentation pattern. A scheme showing the fragmentation pattern of DPPC and the probable fragments cleaved off from the acyl chain and the choline head group.

from the anionic lipid head group and zwitterionic lipid such as DPPC. Therefore, deuterated negatively charged lipids having similar phase behavior to their native counterpart are used in order to differentiate the signals and enhance the ion count. Deuterated DPPG (d62DPPG) with deuterated acyl chain is often used in studies involving pulmonary surfactant model systems. Importantly, the fragmentation pattern of d62DPPG is found to be significantly different from that of DPPC with slightly higher m/z ratio [46]. The masses of M34, M50, M62 and M66, respectively correspond to fragments cleaved off from acyl chains namely $C_2D_5^+$, $C_3D_7^+$, $C_4D_7^+$ and $C_4D_9^+$ [46].

Likewise, proteins also show a peculiar fragmentation pattern characteristic of the amino acid composition. Based on our previous ToF-SIMS studies on lung surfactant model systems, we have especially deciphered few typical SI fragments corresponding to hydrophobic proteins SP-C and SP-B. Since, SP-C is a small protein, it is usually detected as a quasi-molecular ion $(\text{SP-C} + \text{H})^+$ with a characteristic m/z ratio of 4024 u/e in thin film preparations of SP-C formed by spin coater. This quasi-molecular ion is, however, undetectable in LB-layers with lipids [48]. Additionally, specific characteristic fragments of SP-C (for the described model system) are CH_4N^+(Glycine) with m/z of 30 u/e, $C_2H_6N^+$(Alanine) with m/z of 44 u/e and $C_5H_8N_3^+$(Histidine) with m/z of 110 u/e, respectively. Often some of the fragments such as $C_4H_{10}N^+$ and $C_5H_{12}N^+$ with the corresponding m/z of 72 u/e and m/z of 86 u/e interfere with the signals arising from DPPC [48]. Nevertheless, other SI fragments with M18, M30 and M110 are SP-C specific, despite similar DPPC signals, and result in higher intensity which reflects the presence of nitrogen. In general, the most peptide fragments arise as a result of cleavage of the −COOH group of the amino acids: glycine, alanine, valine, leucine/isoleucine, proline and histidine [48]. A similar fragmentation pattern is also obtained for SP-B arising from the respective iminium ions and shared identical fragments with SP-C corresponding to m/z of 44, 70, 72 and 110 u/e. In addition, an SI fragment with M120 could also be detected arising from phenylalanine [46]. An overview of characteristic SI fragments cleaved off various amino acids of proteins is compiled in Table 2. Nevertheless, despite the above overview, care must be taken while interpreting the mass spectra as signals arising from various lipids and protein might often show significant interference [74,75]. Thus, the use of isotopically labeled components becomes essential to avoid interference especially in more complex studies involving native membrane or a complex model system.

Table 1
List of secondary ions obtained from components of surfactant model systems.

m/z	Ion
DPPC	
102	$C_5H_{12}NO^+$
104	$C_5H_{14}NO^+$
125	$C_5H_6NO_4^+$
150	$C_5H_{13}NPO_2^+$
166	$C_5H_{13}NPO_3^+$
184	$C_5H_{15}NPO_4^+$
224	$C_8H_{19}NPO_4^+$
734	$(\text{DPPC}-\text{H})^+$
735	$(\text{DPPC}+\text{H})^+$
DPPG	
173	$C_3H_{10}PO_6^+$
767	$(\text{DPPG}+2\text{Na}-\text{H})^+$
d62DPPG	
34	$C_2D_5^+$
50	$C_3D_7^+$
62	$C_4D_7^+$
66	$C_4D_9^+$
SP-B	
28	CH_2N^+
30	CH_4N^+
44	$C_2H_6N^+$
70	$C_4H_8N^+$
110	$C_5H_8N_3^+/C_7H_{12}N^+$
112	$C_5H_{10}N_3^+/C_7H_{14}N^+$
120	$C_8H_{10}N^+$
SP-C	
18	NH_4^+
30	CH_4N^+
44	$C_2H_6N^+$
110	$C_5H_8N_3^+$
4024	$(\text{SP-C}+\text{H})^+$

Table 2
List of characteristic secondary ions fragments cleaved off from amino acids for mass spectrometric analysis of proteins.

Mass	Ion	Amino acid
30	CH_4N^+	Glycine (Gly, G)
44	$C_2H_6N^+$	Alanine (Ala, A)
60	$C_2H_6NO^+$	Serine (Ser, S)
70	$C_4H_8N^+$	Proline (Pro, P)
72	$C_4H_{10}N^+$	Valine (Val, V)
74	$C_3H_8NO^+$	Threonine (Thr, T)
76	$C_2H_6NS^+$	Cysteine (Cys, C)
86	$C_5H_{12}N^+$	Leucine (Leu, L)
86.1	$C_5H_{12}N^+$	Isoleucine (Ile, I)
87	$C_3H_7N_2O^+$	Aspargine (Asn, N)
88	$C_3H_6NO_2^+$	Aspartate (Asp, D)
101	$C_4H_9N_2O^+$	Glutamine (Gln, Q)
101.1	$C_5H_{13}N_2^+$	Lysine (Lys, K)
102	$C_4H_8NO_2^+$	Glutamate (Glu, E)
104	$C_4H_{10}NS^+$	Methionine (Met, M)
110	$C_5H_8N_3^+$	Histidine (His, H)
120	$C_8H_{10}N^+$	Phenylalanine (Phe, F)
129	$C_5H_{13}N_4^+$	Arginine (Arg, R)
136	$C_8H_{10}NO^+$	Tyrosine (Tyr, Y)
159	$C_{10}H_{11}N_2^+$	Trytophan (Trp, W)

5.2. Chemical imaging of lipid/protein localization in pulmonary surfactant model systems

The molecular mechanism of surfactant proteins remains unclear and there is particular interest in studying their interaction with different lipids, especially at the collapse pressure, where surface confined reservoir is formed. A surface view of membrane structure and dynamics provides us with significant information on the lateral organization of membrane and the eventual spatial and temporal changes that it might undergo. We systematically investigated the membrane lateral organization and the lipid–protein interactions in monolayer model systems. Techniques such as the Langmuir film balance provide basic information about the phase transitions and fluidizing/condensing effects in the membrane. Likewise, fluorescence microscopy allows visualization of the phase separation, domain formation and growth as well as possible condensing or fluidizing effects. However, the interference due to fluorescence probe cannot be ruled out. Additionally, atomic force microscopy gives detailed insights into the topographic features of the phase separated domains. All the above techniques provide us with significant amount of information complimenting the chemical maps obtained from ToF-SIMS. Fig. 5 shows a general schematic representation of different complimentary aspects studied, namely the phase behavior by Langmuir film balance, phase separation and domain formation by fluorescence microscopy, topology of the surface confined reservoir atomic force microscopy and chemical mapping of the lateral organization by ToF-SIMS, that compliment each other.

Electrostatic interactions are believed to exist between cationic surfactant peptides such as SP-B/KL_4 and anionic DPPG, and these interactions are thought to be crucial in lipid/peptide monolayers and to affect lung surfactant function in vivo. Laterally resolved time-of-flight secondary ion mass spectrometry (ToF-SIMS) is unique in itself as it allows for label-free detection of individual compounds of a monolayer (after transfer to a solid support) thereby enabling us to uncover existent specific intermolecular interactions by means of chemical maps displaying distinct areas of colocalized species. In ToF-SIMS analysis, a focused primary ion beam is rastered across a defined area of the sample causing the sputtering of compound-characteristic secondary ions with varying mass-to-charge (m/z) ratios. Pixel by pixel acquisition of the mass spectra of the sputtered ions is then used to map the chemical composition of the sample. Signal intensities for a given secondary ion are mapped such that the brighter regions correspond to high ion counting rates. Thus, the obtained high resolution mass images represent semi-quantitative chemical maps monitoring the lateral localization of the analyzed fragments with a high lateral resolution. We will now review previous studies of the lipid–protein interaction in lung surfactant model systems and our studies performed with ToF-SIMS that aimed to determine the mechanism of action driving the surfactant proteins to either colocalize with anionic DPPG or neutral DPPC.

The first reported study, fluorescence anisotropy, was used to show that, for DPPC/DPPG (7:1) bilayers, SP-B selectively interacts with anionic lipids at pH 7 (120 mM NaCl, 10 mM MOPS) [15]. This work was followed by electron spin resonance spectroscopic studies

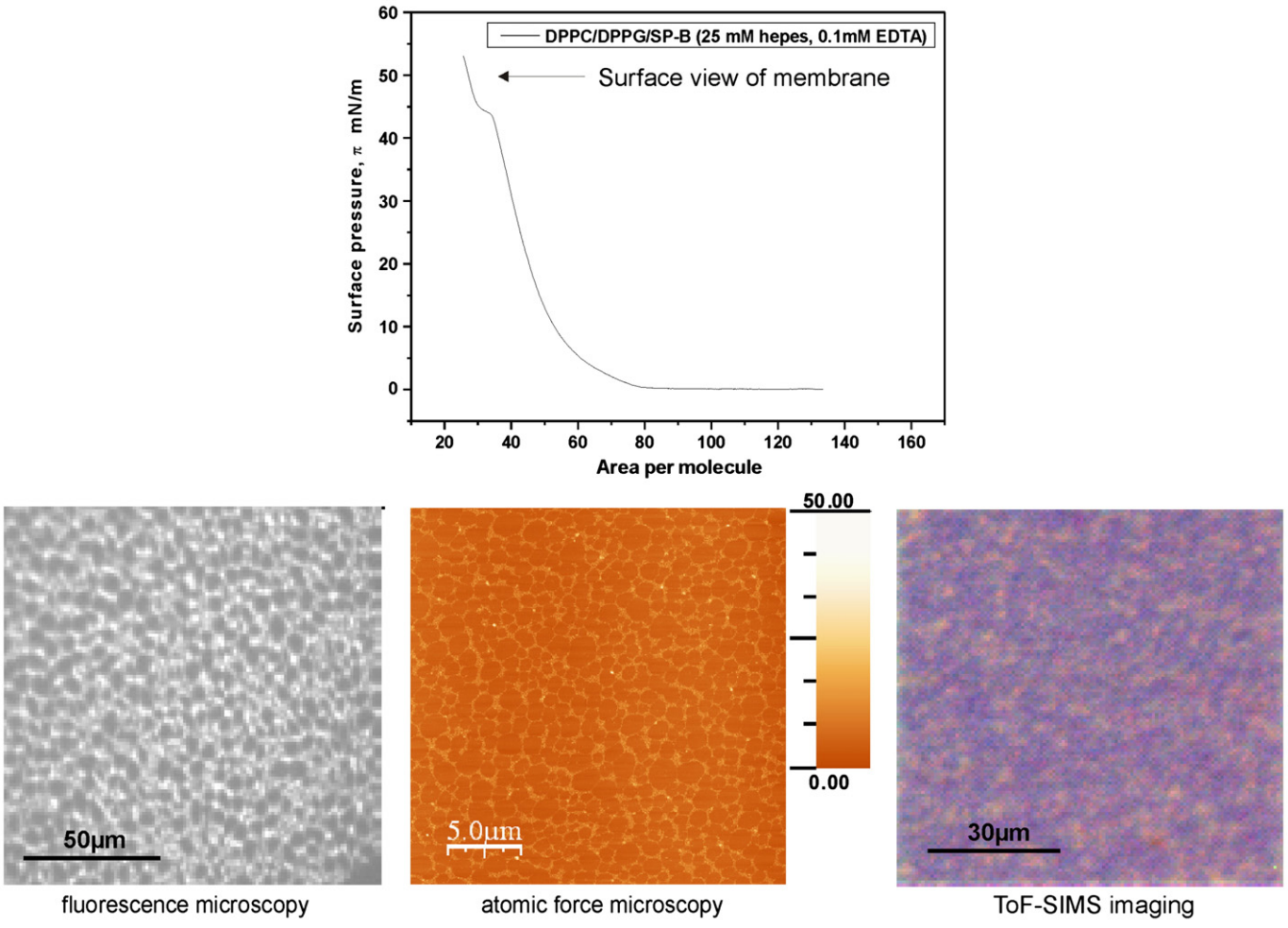

Fig. 5. A general scheme showing the various complementary techniques applied in our studies to characterize domain formation, growth, topology and chemical composition.

on bilayer vesicular systems supporting the idea of the existence of SP-B/DPPG interaction at pH 7 (50 mM HEPES, 150 mM NaCl, 5 mM EDTA) [30]. Interestingly, no such preferential interaction of SP-B with either DPPC or DPPG could be found in bilayers using ^{2}H NMR spectroscopy at pH ~7 (15 mM HEPES, 135 mM NaCl) [31]. As a step, we demonstrated that lipid–protein lateral organization could be imaged laterally. Our first studies on surfactant model systems containing surfactant protein B (i.e., DPPC/DPPG/SP-B), surprisingly showed the colocalization of the zwitterionic DPPC with the surfactant protein forming the domains in an inhomogeneous matrix of negatively charged DPPG [46]. The difference in the pH conditions of the aqueous subphase might have caused this apparent demixing of DPPG and protein. We thus further investigated the effect of pH and carried out a systematic analysis of demixing behavior and lipid–protein colocalization under a range of pH conditions. The investigation using DPPC/DPPG/SP-B monolayers revealed that, both at pH 7.0

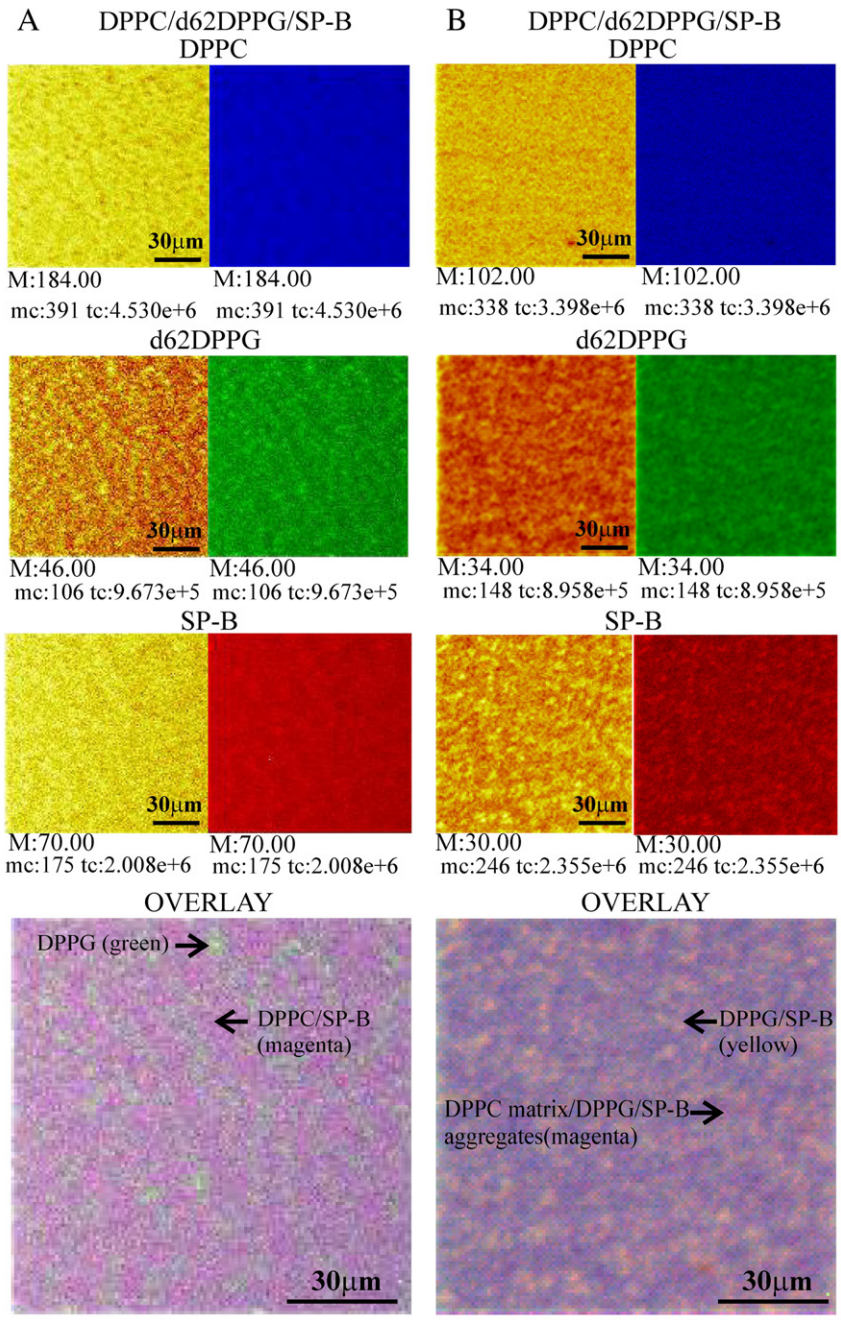

Fig. 6. Mass resolved ToF-SIMS images of surfactant monolayers consisting of (A) DPPC/d62DPPG/SP-B (4:1:0.2 mol%) on aqueous buffer containing traces of calcium. The distributions of positively charged secondary ions deriving from DPPC ($m/z=184$), d62DPPG ($m/z=46$) and SP-B ($m/z=70$) are displayed in characteristic secondary ion intensity maps (*left rows*). Correlation analysis represented by the large three-color overlay image obtained from overlapping the respective secondary ion maps with primary color background (*right rows*), shows the colocalization of the DPPC and SP-B (magenta) network while DPPG forms condensed domains (green). (B) DPPC/d62DPPG/SP-B (4:1:0.2 mol%) on aqueous buffer without calcium. The distributions of positively charged secondary ions deriving from DPPC ($m/z=102$), d62DPPG ($m/z=34$) and SP-B ($m/z=30$) are displayed in characteristic secondary ion intensity maps (*left rows*). Correlation analysis represented by the large three-color overlay image obtained after overlapping the respective secondary ion maps with primary color background (*right rows*), shows the colocalization of DPPG and SP-B appearing as yellow colored domains whereas magenta colored network might reflect a DPPC matrix containing aggregates of DPPG/SP-B. For both images A and B, yellow/bright colored regions suggest a higher intensity count of the secondary ion whereas brown/dark colored regions denote a lower intensity count or absence of the same secondary ion. LB-transfer was performed on gold-covered glass slides at 50 mN/m from a subphase containing buffer with and without calcium at 20 °C.

and 5.5, SP-B colocalizes with the rigidified DPPC-rich phase [59]. It was therefore suggested that an extended hydrogen-bond network of the head group region of DPPG leads to the bridging of adjacent lipid molecules, largely reducing the solubility of SP-B in the DPPG-rich phase. Consequently, the protein would then be excluded from the condensed DPPG domains and colocalize with the surrounding fluid DPPC matrix. However, SP-B/DPPG-specific interaction could not be ruled out. Speculating about the possible role of the ionic conditions of the subphase on observed demixing behavior and assuming that our previous studies had traces of Calcium in the aqueous buffer, we systematically investigated the DPPC/DPPG monolayers containing SP-B and its model peptide KL_4 in the presence and absence of calcium in the subphase [60]. Interestingly, it was observed that there is an apparent reversal of protein colocalization with the DPPG in the absence of calcium in the subphase [32].

Fig. 6. shows the mass-resolved images of DPPC/d62DPPG/SP-B (4:1 molar ratio lipid with 0.2 mol % SP-B) monolayers transferred to solid supports from aqueous buffer containing traces of calcium. These images were obtained in burst alignment mode (focus 300 nm) with a Bi_3^+ primary ion beam. The negatively charged lipid d62DPPG, identified by the secondary ion $C_3D_7^+$ with an m/z value of 46 u/e, was found to form distinct domains with high SI intensity denominated by the bright (*yellow*) regions in a dark network with low secondary ion yields (*brown*). Characteristic signals detected for DPPC and SP-B are attributed to $C_5H_{15}NPO_4^+$ (M184) and $C_4H_8N^+$ (M70), respectively, and were found to possess highest signal intensities in the network surrounding the d62DPPG domains. It was therefore concluded from the obtained distribution pattern that a demixing of the monolayer components has occurred and the protein colocalized with DPPC. A correlation analysis is often desirable for ternary mixtures to unambiguously verify the lateral molecular distribution of all the surfactant compounds with respect to each other. The primary colors *blue*, *green* and *red* were used to depict the chemical maps specific to DPPC, d62DPPG and SP-B, respectively. The lateral organization could be inferred from the respective fusion of the colors of different chemical maps. A superimposition of red and blue would give *magenta* colored regions, red and green would result in *yellow* areas while fusion of blue and green would appear as *cyan*. This mode of evaluation of ToF-SIMS images furnishes a clearer picture of the lateral distribution of different biomolecules. In the case of SP-B containing lipid mixtures, no colocalization of the protein with DPPG was evidenced. Only *magenta* and *green* colored regions appear, clearly showing that DPPC fragments (*blue*) and SP-B secondary ions (*red*) are present in the same phase, whereas d62DPPG (*green*) forms separated domains.

On the contrary, the ToF-SIMS mass resolved images obtained for DPPC/d62DPPG/SP-B (4:1 molar ratio lipid with 0.2 mol % protein) LB-films transferred from subphase in the absence of calcium show that the characteristic signals for DPPC result from cleavages in the lipid head group regions and yield fragments such as $C_5H_{12}NO^+$ with $m/z = 102$ u/e (M102) or $C_5H_{14}NO^+$ with $m/z = 104$ u/e (M104) and these are found to be rather homogeneously distributed over the complete surface of samples. d62DPPG, identifiable by its deuterated acyl chain fragments such as $C_2D_5^+$ (M34) was found in distinct circular domains in monolayers along with SP-B. The protein itself is identifiable by secondary ions originating from the cleavage of COOH from amino acids leading to typical fragments such as $m/z = 30$ u/e (Gly). Furthermore, a similar three-color overlay analysis showed SP-B (red) and DPPG (green) superimposed as yellow colored regions indicative of a colocalization of SP-B and d62DPPG. Additionally, magenta colored regions surrounding yellow colored domain areas were observed that could be attributed to the d62DPPG/SP-B aggregates embedded in the DPPC-rich lipid matrix. Colocalization of the SP-B model peptide KL_4 was similar, further strengthening our hypothesis on the role of fluidity in lipid–protein lateral organization [32,60].

This apparent reversal of the colocalization of SP-B and KL_4 could most easily be explained in terms of the electrostatic interactions existing at the air/water interface modulating the lateral organization of the monolayer. The glycerol-containing lipid head groups have been found to form a dense hydrogen-bonding network that bridges negatively charged lipids, thereby reducing the solubility of SP-B/KL_4 in such densely packed regions [81,82]. Moreover, the strength of this hydrogen bonding network would naturally depend on the interfacial pH and ionic strength. Most importantly, monovalent cations have been found to deeply penetrate into the head-group region of DPPG, thus stabilizing the so-called liquid-expanded(LE) phase of lipid monolayer [83]. It is highly possible that in the presence of NaCl as in previous reports of DPPG/SP-B interaction [15,30] or in the absence of calcium ions [32], DPPG exists in a more fluid state thereby enabling SP-B or KL_4 to interact with the negatively charged head groups via predominant electrostatic interaction.

In conclusion, our ToF-SIMS results show that colocalization of SP-B or KL_4 with certain phospholipids depends on lipid fluidity and the miscibility of respective surfactant components, which in turn depends on the ionic environment. The reversal of the protein colocalization with either DPPC or DPPG thus depends on the presence of calcium ions, which seem to act as a "miscibility switch" and to be one of the major factors deciding the mixing behavior of DPPG in a DPPC/protein matrix. By this we also demonstrate the usefulness of ToF-SIMS technique for investigating the lateral organization of membrane structure and mapping molecular interactions.

Acknowledgements

We would like to thank Tascon GmbH, Münster, Germany, especially Dr. B. Hagenhoff and Dr. D. Breitenstein for their fruitful longstanding collaboration. This work was supported by the NRW Graduate School of Chemistry (to MS) and the Deutsche Forschungsgemeinschaft (DFG) as a contribution from the Sonderforschungsbereich 424/B9 (to HJG).

References

[1] A.D. Bangham, C.J. Morley, M.C. Phillips, The physical properties of an effective lung surfactant, Biochim. Biophys. Acta 573 (1979) 552–556.
[2] S. Yu, P.G. Harding, N. Smith, F. Possmayer, Bovine pulmonary surfactant: chemical composition and physical properties, Lipids 18 (1983) 522–529.
[3] J. Goerke, Lung surfactant, Biochim. Biophys. Acta 344 (1974) 241–261.
[4] L.A. Creuwels, L.M. van Golde, H.P. Haagsman, The pulmonary surfactant system: biochemical and clinical aspects, Lung 175 (1997) 1–39.
[5] Y. Kuroki, D.R. Voelker, Pulmonary surfactant proteins, J. Biol. Chem. 269 (1994) 25943–25946.
[6] S. Hawgood, M. Derrick, F. Poulain, Structure and properties of surfactant protein B, Biochim. Biophys. Acta 1408 (1998) 150–160.
[7] S.H. Yu, F. Possmayer, Lipid compositional analysis of pulmonary surfactant monolayers and monolayer-associated reservoirs, J. Lipid Res. 44 (2003) 621–629.
[8] J. Ma, S. Koppenol, H. Yu, G. Zografi, Effects of a cationic and hydrophobic peptide, KL4, on model lung surfactant lipid monolayers, Biophys. J. 74 (1998) 1899–1907.
[9] M. Gustafsson, G. Vandenbussche, T. Curstedt, J.M. Ruysschaert, J. Johansson, The 21-residue surfactant peptide (LysLeu4)4Lys(KL4) is a transmembrane alpha-helix with a mixed nonpolar/polar surface, FEBS Lett. 384 (1996) 185–188.
[10] C.G. Cochrane, S.D. Revak, T.A. Merritt, G.P. Heldt, M. Hallman, M.D. Cunningham, D. Easa, A. Pramanik, D.K. Edwards, M.S. Alberts, The efficacy and safety of KL4-surfactant in preterm infants with respiratory distress syndrome, Am. J. Respir. Crit. Care Med. 153 (1996) 404–410.
[11] P. Cai, C.R. Flach, R. Mendelsohn, An infrared reflection-absorption spectroscopy study of the secondary structure in (KL4)4K, a therapeutic agent for respiratory distress syndrome, in aqueous monolayers with phospholipids, Biochemistry 42 (2003) 9446–9452.
[12] J. Johansson, M. Gustafsson, M. Palmblad, S. Zaltash, B. Robertson, T. Curstedt, Synthetic surfactant protein analogues, Biol. Neonate 74 (Suppl. 1) (1998) 9–14.
[13] K. Nag, S.G. Taneva, J. Perez-Gil, A. Cruz, K.M. Keough, Combinations of fluorescently labeled pulmonary surfactant proteins SP-B and SP-C in phospholipid films, Biophys. J. 72 (1997) 2638–2650.
[14] K. Nag, K.M. Keough, Epifluorescence microscopic studies of monolayers containing mixtures of dioleoyl- and dipalmitoylphosphatidylcholines, Biophys. J. 65 (1993) 1019–1026.
[15] J.E. Baatz, B. Elledge, J.A. Whitsett, Surfactant protein SP-B induces ordering at the surface of model membrane bilayers, Biochemistry 29 (1990) 6714–6720.

[16] M.A. Oosterlaken-Dijksterhuis, M. van Eijk, L.M. van Golde, H.P. Haagsman, Lipid mixing is mediated by the hydrophobic surfactant protein SP-B but not by SP-C, Biochim. Biophys. Acta 1110 (1992) 45–50.
[17] C.G. Cochrane, S.D. Revak, Pulmonary surfactant protein B (SP-B): structure–function relationships, Science 254 (1991) 566–568.
[18] V.K. Sarin, S. Gupta, T.K. Leung, V.E. Taylor, B.L. Ohning, J.A. Whitsett, J.L. Fox, Biophysical and biological activity of a synthetic 8.7-kDa hydrophobic pulmonary surfactant protein SP-B, Proc. Natl. Acad. Sci. U. S. A. 87 (1990) 2633–2637.
[19] R. Bruni, H.W. Taeusch, A.J. Waring, Surfactant protein B: lipid interactions of synthetic peptides representing the amino-terminal amphipathic domain, Proc. Natl. Acad. Sci. U. S. A. 88 (1991) 7451–7455.
[20] K. Nag, J. Perez-Gil, M.L. Ruano, L.A. Worthman, J. Stewart, C. Casals, K.M. Keough, Phase transitions in films of lung surfactant at the air–water interface, Biophys. J. 74 (1998) 2983–2995.
[21] R. Veldhuizen, K. Nag, S. Orgeig, F. Possmayer, The role of lipids in pulmonary surfactant, Biochim. Biophys. Acta 1408 (1998) 90–108.
[22] A.M. Cockshutt, D.R. Absolom, F. Possmayer, The role of palmitic acid in pulmonary surfactant: enhancement of surface activity and prevention of inhibition by blood proteins, Biochim. Biophys. Acta 1085 (1991) 248–256.
[23] B.A. Holm, Z. Wang, E.A. Egan, R.H. Notter, Content of dipalmitoyl phosphatidylcholine in lung surfactant: ramifications for surface activity, Pediatr. Res. 39 (1996) 805–811.
[24] Z. Wang, S.B. Hall, R.H. Notter, Dynamic surface activity of films of lung surfactant phospholipids, hydrophobic proteins, and neutral lipids, J. Lipid Res. 36 (1995) 1283–1293.
[25] Y. Tanaka, T. Takei, Y. Kanazawa, Lung surfactants: II. Effects of fatty acids, triacylglycerols and protein on the activity of lung surfactant, Chem. Pharm. Bull. (Tokyo) 31 (1983) 4100–4109.
[26] S. Hawgood, K. Shiffer, Structures and properties of the surfactant-associated proteins, Annu. Rev. Physiol. 53 (1991) 375–394.
[27] J. Johansson, T. Curstedt, B. Robertson, The proteins of the surfactant system, Eur. Respir. J. 7 (1994) 372–391.
[28] J. Johansson, T. Curstedt, Molecular structures and interactions of pulmonary surfactant components, Eur. J. Biochem. 244 (1997) 675–693.
[29] H. Sano, Y. Kuroki, The lung collectins, SP-A and SP-D, modulate pulmonary innate immunity, Mol. Immunol. 42 (2005) 279–287.
[30] J. Perez-Gil, C. Casals, D. Marsh, Interactions of hydrophobic lung surfactant proteins SP-B and SP-C with dipalmitoylphosphatidylcholine and dipalmitoylphosphatidylglycerol bilayers studied by electron spin resonance spectroscopy, Biochemistry 34 (1995) 3964–3971.
[31] A.S. Dico, J. Hancock, M.R. Morrow, J. Stewart, S. Harris, K.M. Keough, Pulmonary surfactant protein SP-B interacts similarly with dipalmitoylphosphatidylglycerol and dipalmitoylphosphatidylcholine in phosphatidylcholine/phosphatidylglycerol mixtures, Biochemistry 36 (1997) 4172–4177.
[32] M. Saleem, M.C. Meyer, D. Breitenstein, H.J. Galla, Calcium ions as “miscibility switch”: colocalization of surfactant protein B with anionic lipids under absolute calcium free conditions, Biophys. J. 97 (2009) 500–508.
[33] A. Benninghoven, Chemical analysis of inorganic and organic surfaces and thin films by static time-of-flight secondary ion mass spectrometry (TOF-SIMS), Angewandte Chemie, International Edition in English 33 (1994) 1023–1043.
[34] A. Brunelle, D. Touboul, O. Laprevote, Biological tissue imaging with time-of-flight secondary ion mass spectrometry and cluster ion sources, J. Mass Spectrom. 40 (2005) 985–999.
[35] B. Hagenhoff, A. Benninghoven, J. Spinke, M. Liley, W. Knoll, Time-of-flight secondary ion mass spectrometry investigations of self-assembled monolayers of organic thiols, sulfides, and disulfides on gold surfaces, Langmuir 9 (1993) 1622–1624.
[36] R.N. Sodhi, Time-of-flight secondary ion mass spectrometry (TOF-SIMS): versatility in chemical and imaging surface analysis, Analyst 129 (2004) 483–487.
[37] H. Nygren, K. Borner, B. Hagenhoff, P. Malmberg, J.E. Mansson, Localization of cholesterol, phosphocholine and galactosylceramide in rat cerebellar cortex with imaging TOF-SIMS equipped with a bismuth cluster ion source, Biochim. Biophys. Acta 1737 (2005) 102–110.
[38] A.M. Belu, D.J. Graham, D.G. Castner, Time-of-flight secondary ion mass spectrometry: techniques and applications for the characterization of biomaterial surfaces, Biomaterials 24 (2003) 3635–3653.
[39] M.C. Biesinger, P.Y. Paepegaey, N.S. McIntyre, R.R. Harbottle, N.O. Petersen, Principal component analysis of TOF-SIMS images of organic monolayers, Anal. Chem. 74 (2002) 5711–5716.
[40] R. Van Ham, L. Van Vaeck, A. Adriaens, F. Adams, B. Hodgesc, G. Groenewold, Inorganic speciation in static SIMS: a comparative study between monatomic and polyatomic primary ions, J. Anal. At. Spectrom. 17 (2002) 753–758.
[41] J. Cheng, N. Winograd, Depth profiling of peptide films with TOF-SIMS and a C-60 probe, Anal. Chem. 77 (2005) 3651–3659.
[42] B. Hagenhoff, High resolution surface analysis by TOF-SIMS, Mikrochim. Acta 132 (2000) 259–271.
[43] Michael Seifert, Mohammed Saleem, Daniel Breitenstein, Hans-Joachim Galla, M. C. Meyer, Structure and Dynamics of Membranous Interfaces—ToF-SIMS imaging of lipid/protein model systems, Wiley, 2008.
[44] S.G. Boxer, M.L. Kraft, P.K. Weber, Advances in imaging secondary ion mass spectrometry for biological samples, Annu. Rev. Biophys. 38 (2009) 53–74.
[45] A.G. Sostarecz, D.M. Cannon Jr., C.M. McQuaw, S. Sun, A.G. Ewing, N. Winograd, Influence of molecular environment on the analysis of phospholipids by time-of-flight secondary ion mass spectrometry, Langmuir 20 (2004) 4926–4932.
[46] D. Breitenstein, J.J. Batenburg, B. Hagenhoff, H.J. Galla, Lipid specificity of surfactant protein B studied by time-of-flight secondary ion mass spectrometry, Biophys. J. 91 (2006) 1347–1356.
[47] M.L. Pacholski, N. Winograd, Imaging with mass spectrometry, Chem. Rev. 99 (1999) 2977–3005.
[48] N. Bourdos, F. Kollmer, A. Benninghoven, M. Ross, M. Sieber, H.J. Galla, Analysis of lung surfactant model systems with time-of-flight secondary ion mass spectrometry, Biophys. J. 79 (2000) 357–369.
[49] N. Bourdos, F. Kollmer, A. Benninghoven, M. Sieber, H.-J. Galla, Imaging of domain structures in a one-component lipid monolayer by time-of-flight secondary ion mass spectrometry, Langmuir 16 (2000) 1481–1484.
[50] A. von Nahmen, A. Post, H.J. Galla, M. Sieber, The phase behavior of lipid monolayers containing pulmonary surfactant protein C studied by fluorescence light microscopy, Eur. Biophys. J. 26 (1997) 359–369.
[51] M. Ross, C. Steinem, H.-J. Galla, A. Janshoff, Visualization of chemical and physical properties of calcium-induced domains in DPPC/DPPS Langmuir-Blodgett layers, Langmuir 17 (2001) 2437–2445.
[52] S. Chandra, G.H. Morrison, Sample preparation of animal tissues and cell cultures for secondary ion mass spectrometry (SIMS) microscopy, Biol. Cell 74 (1992) 31–42.
[53] J.L. Guerquin-Kern, T.D. Wu, C. Quintana, A. Croisy, Progress in analytical imaging of the cell by dynamic secondary ion mass spectrometry (SIMS microscopy), Biochim. Biophys. Acta 1724 (2005) 228–238.
[54] C.P. Lechene, Y. Luyten, G. McMahon, D.L. Distel, Quantitative imaging of nitrogen fixation by individual bacteria within animal cells, Science 317 (2007) 1563–1566.
[55] M. Edidin, The state of lipid rafts: from model membranes to cells, Annu. Rev. Biophys. Biomol. Struct. 32 (2003) 257–283.
[56] A. Benninghoven, W. Sichtermann, Detection, identification and structural investigation of biologically important compounds by secondary ion mass spectrometry, Anal. Chem. 50 (1978) 1180–1184.
[57] H.U. Jabs, G. Assmann, D. Greifendorf, A. Benninghoven, High performance liquid chromatography and time-of-flight secondary ion mass spectrometry: a new dimension in structural analysis of apolipoproteins, J. Lipid. Res. 27 (1986) 613–621.
[58] A.v. Eckardstein, H. Funke, M. Walter, K. Altland, A. Benninghoven, G. Assmann, Structural analysis of human apolipoprotein A-I variants. Amino acid substitutions are nonrandomly distributed throughout the apolipoprotein A-I primary structure, J. Biol. Chem. 265 (1990) 8610–8617.
[59] M. Seifert, D. Breitenstein, U. Klenz, M.C. Meyer, H.J. Galla, Solubility versus electrostatics: what determines lipid/protein interaction in lung surfactant, Biophys. J. 93 (2007) 1192–1203.
[60] M. Saleem, M.C. Meyer, D. Breitenstein, H.J. Galla, The surfactant peptide KL4 in lipid monolayers: phase behavior, topography, and chemical distribution, J. Biol. Chem. 283 (2008) 5195–5207.
[61] K.M. Leufgen, H. Rulle, A. Benninghoven, M. Sieber, H.-J. Galla, Imaging time-of-flight secondary ion mass spectrometry allows visualization and analysis of coexisting phases in Langmuir–Blodgett films, Langmuir 12 (1996) 1708–1711.
[62] M.C. Biesinger, D.J. Miller, R.R. Harbottle, F. Possmayer, N.S. McIntyre, N.O. Petersen, Imaging lipid distributions in model monolayers by TOF-SIMS with selectively deuterated components and principal component analysis, Appl. Surf. Sci. 252 (2006) 6065–6957.
[63] L. Zheng, A. Wucher, N. Winograd, Fundamental studies of molecular depth profiling and 3D imaging using Langmuir–Blodgett films as a model, Appl. Surf. Sci. 255 (2008) 816–818.
[64] L. Zheng, C.M. McQuaw, M.J. Baker, N.P. Lockyer, J.C. Vickerman, A.G. Ewing, N. Winograd, Investigating lipid–lipid and lipid–protein interactions in model membranes by ToF-SIMS, Appl. Surf. Sci. 255 (2008) 1190–1192.
[65] M.J. Baker, L. Zheng, N. Winograd, N.P. Lockyer, J.C. Vickerman, Mass spectral imaging of glycophospholipids, cholesterol, and glycophorin a in model cell membranes, Langmuir 24 (2008) 11803–11810.
[66] C.M. McQuaw, L. Zheng, A.G. Ewing, N. Winograd, Localization of sphingomyelin in cholesterol domains by imaging mass spectrometry, Langmuir 23 (2007) 5645–5650.
[67] M.L. Kraft, P.K. Weber, M.L. Longo, I.D. Hutcheon, S.G. Boxer, Phase separation of lipid membranes analyzed with high-resolution secondary ion mass spectrometry, Science 313 (2006) 1948–1951.
[68] T.P. Roddy, D.M. Cannon Jr., C.A. Meserole, N. Winograd, A.G. Ewing, Imaging of freeze-fractured cells with in situ fluorescence and time-of-flight secondary ion mass spectrometry, Anal. Chem. 74 (2002) 4011–4019.
[69] S. Parry, N. Winograd, High-resolution TOF-SIMS imaging of eukaryotic cells preserved in a trehalose matrix, Anal. Chem. 77 (2005) 7950–7957.
[70] T.L. Colliver, C.L. Brummel, M.L. Pacholski, F.D. Swanek, A.G. Ewing, N. Winograd, Atomic and molecular imaging at the single-cell level with TOF-SIMS, Anal. Chem. 69 (1997) 2225–2231.
[71] H. Nygren, B. Hagenhoff, P. Malmberg, M. Nilsson, K. Richter, Bioimaging TOF-SIMS: High resolution 3D imaging of single cells, Microsc. Res. Tech. 70 (2007) 969–974.
[72] S.G. Ostrowski, C.T. Van Bell, N. Winograd, A.G. Ewing, Mass spectrometric imaging of highly curved membranes during Tetrahymena mating, Science 305 (2004) 71–73.
[73] D. Breitenstein, C.E. Rommel, R. Mollers, J. Wegener, B. Hagenhoff, The chemical composition of animal cells and their intracellular compartments reconstructed from 3D mass spectrometry, Angew Chem. Int. Ed. Engl. 46 (2007) 5332–5335.
[74] J.G. Newmann, B.A. Carlson, R.S. Michael, J.F. Moulder, A.H. Teresa, Static SIMS Handbook of Polymer Analysis, Perkin-Elmer Corp., 1991

[75] D. Briggs, A. Brown, J.C. Vickermann, Handbook of Static Secondary Ion Mass Spectrometry (SIMS), Wiley, UK, 1989.
[76] E. Ayanoglu, A. Wegmann, O. Pilet, G.D. Marbury, J.R. Hass, C. Djerassi, Mass spectrometry of phospholipids. Some applications of desorption chemical ionization and fast atom bombardment, J. Am. Chem. Soc. 106 (1984) 5246–5251.
[77] T. Matsuhara, A. Hayashi, FAB/mass spectrometry of lipids, Prog. Lipid Res. 30 (1991) 301–322.
[78] D.J. Harvey, Matrix-assisted laser desorption/ionization mass spectrometry of phospholipids, J. Mass Spectrom. 30 (1995) 1333–1346.
[79] N. Bourdos, F. Kollmer, A. Benninghoven, M. Ross, M. Sieber, H.-J. Galla, Analysis of lung surfactant model systems with time-of-flight secondary ion mass spectrometry, Biophys. J. 79 (2000) 357–369.
[80] N. Bourdos, F. Kollmer, A. Benninghoven, M. Sieber, H.J. Galla, Imaging of domain structures in a one-component lipid monolayer by time-of-flight secondary ion mass spectrometry, Langmuir 16 (2000) 1481–1484.
[81] A. Blume, W. Hubner, G. Messner, Fourier transform infrared spectroscopy of 13C = O-labeled phospholipids hydrogen bonding to carbonyl groups, Biochemistry 27 (1988) 8239–8249.
[82] A. Dicko, T. Di Paolo, M. Pezolet, Interaction of dehydroepiandrosterone with phospholipid membranes: an infrared spectroscopy investigation, Biochim. Biophys. Acta 1368 (1998) 321–328.
[83] E. Maltseva, V.L. Shapovalov, H. Mohwald, G. Brezesinski, Ionization state and structure of l-1,2-dipalmitoylphosphatidylglycerol monolayers at the liquid/air interface, J. Phys. Chem. B 110 (2006) 919–926.